ACADEMIC PRESS

Available online at www.sciencedirect.com

SCIENCE DIRECT®

Journal of Sound and Vibration 270 (2004) 207–231

JOURNAL OF SOUND AND VIBRATION

www.elsevier.com/locate/jsvi

A numerical method for the computation of the resonance frequencies and modes of a fluid-loaded plate: application to the transient response of the system

D. Habault[a,*], P.J.T. Filippi[b]

[a] *CNRS-Laboratoire de Mécanique et d'Acoustique, 31 chemin Joseph Aiguier, 13402 Marseille cedex 20, France*
[b] *La Santa Severa, CNPRS–Appontement 10, Port de la Pointe Rouge, 13008 Marseille, France*

Received 2 May 2002; accepted 8 January 2003

Abstract

In previous papers, we have shown that the time response of a fluid-loaded structure can be expressed in terms of the resonance modes of the fluid/structure system. We first show the efficiency of such a representation by comparing numerical predictions to experimental results. The main objective of this paper is to consider the numerical aspects of this representation, namely the computation of the coupling term in the variational equation and the computation of the resonance frequencies and modes. Three methods are proposed to compute the resonance frequencies: an iterative technique, a Warburton approximation and a perturbation technique (light fluid approximation). Numerical results are presented to compare these three methods, for air and water-loading. The last part of the paper discusses the choice of the number of resonance modes which is required to obtain a representation of the transient radiated pressure with a sufficient accuracy.

1. Introduction

In two previous papers [1,2], the authors showed how resonance modes can be used to express the sound and vibratory behaviour of a structure immersed in a fluid. They proposed an example which demonstrates that the resonance modes are quite convenient to describe the time response of the fluid/structure system. It was a comparison between numerical and experimental results, obtained in the case of a finite length cylindrical thin shell, with hemispherical end caps, immersed in water.

*Corresponding author. Tel.: +33-4-91-16-40-69; fax: +33-4-91-16-40-80.
E-mail address: habault@lma.cnrs-mrs.fr (D. Habault).

0022-460X/03/$ - see front matter
doi:10.1016/S0022-460X(03)00491-7

In this paper, we present the example of a baffled thin plate, with clamped boundaries, hit by a small elastic sphere. The experimental plate is clamped in an aperture which connects two anechoic rooms. The numerical predictions are obtained as a series of the fluid-loaded resonance modes of the plate, computed as described here.

This work is focused on the numerical aspects of the representation based on resonance modes. Three problems are apparent. The first one is the computation of the coupling term in the variational equation. The second one is the computation of the resonance frequencies and modes of the fluid-loaded structure. The last one is the study of some criteria to choose the number of modes to be taken into account to obtain the time acoustic pressure radiated by the structure with a sufficient accuracy. We must mention that our approach is similar to the method proposed in Ref. [3].

The algorithms are developed on the example of a rectangular fluid-loaded baffled plate for its simplicity. But they can be rather easily adapted to more complex structures, in particular, for the numerical approximation of the coupling term.

The first aspect studied in this paper is the computation of the coupling term—corresponding to the acoustic pressure exerted by the fluid on the plate—which, in particular, governs the structural damping due to acoustic radiation. With the algorithm proposed, the accuracy of the numerical approximation can be correctly estimated. In the variational equations, the coupling term is a quadruple integral of the product of a Green's kernel by two basis functions. The difficulty in obtaining an accurate integration is due to the Green's kernel singularity and to the oscillatory properties of the three functions involved. This has been already discussed in several papers (see Refs. [4–7], for example). But, in our opinion, the numerical approximation proposed here is somewhat new, the accuracy can be easily controlled and the numerical algorithm is rather fast.

The second aspect is the computation of the resonance frequencies and modes. Three methods are proposed here. The resonance modes are sought as an expansion into a series of basis functions conveniently chosen. The variational equations lead to an infinite system of equations which must be truncated. The most accurate numerical method for computing the resonance modes is based on an iterative technique and applies to any kind of fluid loading (gas or liquid as well). The second method is a Warburton type approximation which accounts for the diagonal terms only; its advantage is to reduce the computing time. The third method is a perturbation technique (light fluid approximation) which applies for weak loadings (when the fluid is typically a gas) and was developed in a former paper [8]; it is the less time-consuming numerical approximation.

The content of this paper is as follows. Section 2 briefly recalls the basic equations which govern the motion of a fluid-loaded baffled plate, the definition of the resonance frequencies and resonance modes and presents the series expansion of the solution (plate displacement and radiated acoustic pressure) in terms of the resonance modes. The comparison between numerical and experimental results shows the efficiency of the method. Section 3 is dedicated to the numerical computation of the various terms which appear in the equations. In particular, the approximation of the coupling term is described in some details and its numerical accuracy is shown. In Section 4 three methods are described to compute the resonance frequencies and modes. Numerical results are presented in Section 5. The convergence of the iterative procedure, used to solve the exact system of equations, is shown. Two other series of results are obtained with the Warburton approximation and with the light-fluid approximation; they are compared with

those given by the first method which is the more accurate. Section 6 is concerned with the choice of the number of modes to be taken into account in the computation. An experimental criterion is proposed.

2. Statement of the problem—response of a fluid-loaded baffled plate

Let us consider a thin elastic plate occupying a domain Σ, with boundary $\partial\Sigma$, of the $z = 0$ plane; it is extended by a perfectly rigid baffle which occupies the plane complement $\bar{\Sigma}$ of Σ (see Fig. 1). The domain Ω, composed of the two half-spaces $z > 0$ and $z < 0$, is occupied by a perfect fluid. The plate has a thickness $h(x, y) = h_0(1 + \varepsilon(x, y))$ which may vary around a constant value h_0 by a small amount ε. The plate material has a density μ, Young's modulus E, a Poisson ratio ν; the plate rigidity is $D = Eh^3/12(1 - \nu^2)$. The fluid is characterized by a density μ_0 and a sound speed c_0. The boundary condition along $\partial\Sigma$ will be specified later. For simplicity, it is assumed that the only energy source is a mechanical real force $\tilde{F}(M, t) = \tilde{\psi}(t)f(M)$ acting on the plate, which is zero for $t < 0$. The system is assumed to be at rest for $t < 0$.

2.1. Basic equations

Here, we use the most classical equations for the plate motion and the acoustic field. In particular, the structure and the fluid are supposed to have no damping (see, for example Refs. [9–11]). If more accurate equations are necessary (damping in the fluid and/or in the material, orthotropic material, etc.), the method proposed here remains unchanged.

The unknown functions of the problem are $\tilde{W}(M, t)$ the plate displacement and $\tilde{P}(Q, t)$ the acoustic pressure. In rectangular co-ordinates, the governing equations are given by

$$\left(\Delta - \frac{1}{c_0^2}\frac{\partial^2}{\partial t^2}\right)\tilde{P} = 0 \quad \text{in } \Omega,$$

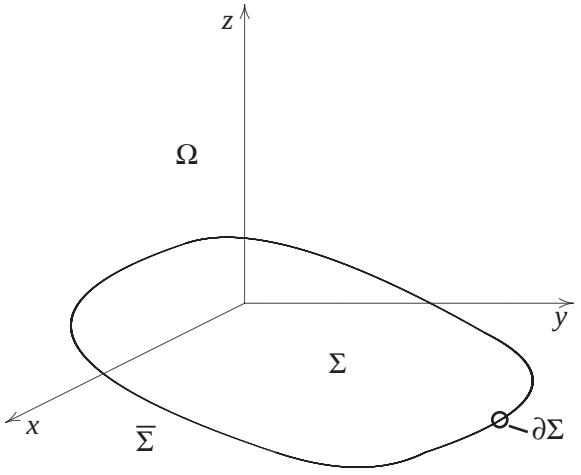

Fig. 1. Sketch of the baffled fluid-loaded plate.

$$\left(\mathscr{D} + \mu h \frac{\partial^2}{\partial t^2}\right)\tilde{W} + \tilde{\tilde{P}} = \tilde{F} \quad \text{on } \Sigma$$

$$\text{with} \quad \mathscr{D}\tilde{W} := \Delta(D\Delta\tilde{W}) + 2\frac{\partial^2}{\partial x \partial y}\left((1-\nu)D\frac{\partial^2}{\partial x \partial y}\tilde{W}\right) - \frac{\partial^2}{\partial y^2}\left((1-\nu)D\frac{\partial^2}{\partial x^2}\tilde{W}\right) - \frac{\partial^2}{\partial x^2}\left((1-\nu)D\frac{\partial^2}{\partial y^2}\tilde{W}\right), \tag{1}$$

where Δ is the Laplacian operator and $\tilde{\tilde{P}} = Tr^+\tilde{P} - Tr^-\tilde{P}$ is the jump of the acoustic pressure across $z = 0$. The definitions of the symbols are listed in Appendix A. The plate operator $\mathscr{D}$ reduces to $D\Delta^2$ if thickness is constant ($\varepsilon \equiv 0$). An additional equation is provided by the continuity conditions on the plane $z = 0$:

$$\frac{\partial \tilde{P}}{\partial z} = \begin{cases} -\mu_0 \dfrac{\partial^2 \tilde{W}}{\partial t^2} & \text{on } \Sigma, \\ 0 & \text{on } \bar{\Sigma}. \end{cases} \tag{2}$$

Finally, the uniqueness of the solution is ensured by imposing the acoustic pressure to satisfy an outgoing wave condition.

Let $\tilde{\mathscr{G}}(S, Q; t)$ be the Green function of the wave equation which satisfies the homogeneous Neumann condition on the plane $z = 0$ and the outgoing wave condition.

$$\tilde{\mathscr{G}}(S, Q; t) = -\frac{\delta(t - R/c)}{R} - \frac{\delta(t - R'/c)}{R'}, \tag{3}$$

where $R = R(S, Q)$ and $R' = R(S', Q)$, S is the point source and S', its image through $z = 0$. The radiated sound pressure can thus be expressed in terms of the plate displacement as

$$\begin{aligned} \tilde{P}(Q, t) &= -\mu_0 \kappa \tilde{\mathscr{G}} \underset{(Q,t)}{*} \left(\frac{\partial^2 \tilde{W}}{\partial t^2} \otimes \delta_\Sigma\right) \\ &:= -\mu_0 \kappa \int_0^\infty \mathrm{d}t' \int_\Sigma \tilde{\mathscr{G}}(Q, M'; t - t') \frac{\partial^2 \tilde{W}(M', t')}{\partial t'^2} \mathrm{d}M', \end{aligned} \tag{4}$$

where the symbol $\underset{(Q,t)}{*}$ stands for the convolution product over the time and space variables; δ_Σ is the Dirac measure on Σ; and $\kappa = 1$ in $z > 0$ and -1 in $z < 0$. Introducing this relationship in the second equation of Eq. (1) leads to an integrodifferential equation for the plate displacement only:

$$\left(\mathscr{D} + \mu h \frac{\partial^2}{\partial t^2}\right)\tilde{W} - 2\mu_0 \tilde{\mathscr{G}} \underset{(M,t)}{*} \left(\frac{\partial^2 \tilde{W}}{\partial t^2} \otimes \delta_\Sigma\right) = \tilde{F}. \tag{5}$$

2.2. Eigenmodes and resonance modes of the fluid-loaded plate

In a recent paper [1], the authors and their co-authors have developed the concepts of eigenvalues—eigenmodes and of resonance frequencies—resonance modes for a fluid-loaded

structure. We just recall here the corresponding definitions together with the formal series expansions of the response of the plate (displacement and radiated pressure) in the time domain.

Let $\theta(\omega)$ denote the time Fourier transform of any function $\tilde{\theta}(t)$ defined by

$$\theta(\omega) = \int_{-\infty}^{+\infty} \tilde{\theta}(t) \mathrm{e}^{\mathrm{i}\omega t}\, \mathrm{d}t. \tag{6}$$

The Fourier transform of the Green function $\tilde{\mathscr{G}}$ will be denoted by $\mathscr{G}_\omega$:

$$\mathscr{G}_\omega(S, Q) = -\frac{\exp(\mathrm{i}kR)}{4\pi R} - \frac{\exp(\mathrm{i}kR')}{4\pi R'}, \tag{7}$$

where $k = \omega/c_0$. The fluid-loaded plate equation becomes

$$\mathscr{D}W - \mu h\omega^2 W + 2\mu_0\omega^2 \mathscr{G}_\omega \underset{M}{*}(W \otimes \delta_\Sigma) = f\psi$$
$$\text{with} \quad \mathscr{G}_\omega \underset{Q}{*}(W \otimes \delta_\Sigma) \coloneqq \int_\Sigma \mathscr{G}_\omega(Q, M') W(M')\, \mathrm{d}M' \tag{8}$$

($\underset{Q}{*}$ stands for the space convolution product). In the following, use is made of the variational form of Eq. (8). Let us recall that the plate displacement belongs to the functional space, say $\mathbf{H}(\Sigma)$, of functions which are square integrable over Σ, together with their derivatives up to order 2, and which satisfy the given boundary conditions along $\partial\Sigma$. Let U stand for any basis function of $\mathbf{H}(\Sigma)$. The variational form of Eq. (8) is

$$\mathscr{A}(W, U) - \mu h_0 \omega^2 \left[\int_\Sigma (1+\varepsilon) W U^* - \frac{\mu_0}{\mu h_0} \beta_\omega(W, U) \right] = \psi(\omega) \int_\Sigma f\, U^*$$

with

$$\mathscr{A}(W, U) = \int_\Sigma D \left[\left(\frac{\partial^2 W}{\partial x^2} + \frac{\partial^2 W}{\partial y^2} \right) \left(\frac{\partial^2 U^*}{\partial x^2} + \frac{\partial^2 U^*}{\partial y^2} \right) + (1-\nu) \left(2 \frac{\partial^2 W}{\partial x \partial y} \frac{\partial^2 U^*}{\partial x \partial y} - \frac{\partial^2 W}{\partial x^2} \frac{\partial^2 U^*}{\partial y^2} - \frac{\partial^2 W}{\partial y^2} \frac{\partial^2 U^*}{\partial x^2} \right) \right],$$

$$\beta_\omega(W, U) = 2 \int \int_\Sigma W(M) \mathscr{G}_\omega(M, M') U^*(M'). \tag{9}$$

U^* is the complex conjugate of U. β_ω describes the coupling between plate and fluid ($\beta_\omega = 0$, for a plate in vacuo).

The eigenmodes $\hat{W}_n$ and the eigenvalues Λ_n, with $n = \ldots, -1, 1, \ldots$ of the fluid-loaded plate operator are the non-zero solutions to the homogeneous equation

$$\mathscr{A}(\hat{W}_n, U) - \Lambda_n \left[\int_\Sigma (1+\varepsilon) \hat{W}_n U^* - \frac{\mu_0}{\mu h_0} \beta_\omega(\hat{W}_n, U) \right]. \tag{10}$$

They are frequency dependent because the coupling term β_ω depends on ω.

The resonance modes W_n and the resonance angular frequencies ω_n are the non-zero solutions to the homogeneous equation

$$\mathscr{A}(W_n, U) - \mu h_0 \omega_n^2 \left[\int_\Sigma (1+\varepsilon) W_n U^* - \frac{\mu_0}{\mu h_0} \beta_{\omega_n}(W_n, U) \right] = 0. \tag{11}$$

It is useful to associate them by pairs numbered $-n$ and $+n$ because they have the following property [1,12]:

$$\omega_n = \Omega_n - \mathrm{i}\tau_n \quad \text{with } \Omega_n > 0, \qquad \tau_n > 0, \qquad \omega_{-n} = -\omega_n^* \tag{12}$$

and the corresponding resonance modes are complex conjugate.

Let $(U_m, m = 1, 2, \ldots)$ be a basis of the space $\mathbf{H}(\Sigma)$. Each resonance mode can be sought as a series of these basis functions:

$$W_n(M) = \sum_{m=1}^{\infty} u_n^m U_m(M). \tag{13}$$

Eq. (11) leads to the following infinite system of equations:

$$\sum_{m=1}^{\infty} u_n^m \left\{ \mathscr{A}(U_m, U_q^*) - \mu h_0 \omega_n^2 \left[\int_\Sigma (1+\varepsilon) U_m U_q - \frac{\mu_0}{\mu h_0} \beta_{\omega_n}(U_m, U_q^*) \right] \right\} = 0,$$
$$q = 1, 2, \ldots, +\infty. \tag{14}$$

This system of linear algebraic equations has non-zero solutions if ω_n is a resonance angular frequency. In standard eigenvalue problems, the system of equations to be solved is of the form

$$\mathbf{A}\vec{\mathbf{u}} = \Lambda \mathbf{B}\vec{\mathbf{u}}, \tag{15}$$

where $\mathbf{A}$ and $\mathbf{B}$ are two square matrices independent of Λ. System (14) is of the form

$$\mathbf{A}\vec{\mathbf{u}} = \Lambda[\mathbf{B} + \mathbf{C}(\Lambda)]\vec{\mathbf{u}}. \tag{16}$$

Because the matrix $\mathbf{C}$ depends on the eigenvalue, the classical methods for solving eigenvalue problems cannot be used in a straightforward way.

2.3. Response of the fluid-loaded plate

The transient displacement of the plate has the following expansion in terms of the resonance modes (see Ref. [2]):

$$\tilde{W}(M,t) = -\mathrm{i}\tilde{\psi}(t) \underset{t}{*} Y(t) \sum_{n=1}^{\infty} \left[\frac{\langle f, W_n^* \rangle}{\Lambda_n'(\omega_n) - 2\mu h \omega_n} W_n(M) \mathrm{e}^{-\mathrm{i}\omega_n t} - \frac{\langle f, W_n^* \rangle^*}{\Lambda_n'^*(\omega_n) - 2\mu h \omega_n^*} W_n^*(M) \mathrm{e}^{+\mathrm{i}\omega_n^* t} \right], \tag{17}$$

where $\underset{t}{*}$ denotes the time convolution product. This expression is, of course, valid for $t > 0$ only.

By introducing formula (17) into expression (4), one gets the following series:

$$\tilde{P}(M,t) = \mathrm{sgn}(z)\mu_0 \tilde{\mathscr{G}}(M,t) \underset{(M,t)}{*} \frac{\partial^2}{\partial t^2}\left\{ -\mathrm{i}\tilde{\psi}(t) \underset{t}{*} Y(t) \right.$$
$$\left. \sum_{n=1}^{\infty}\left[\frac{\langle f, W_n^* \rangle}{\Lambda_n'(\omega_n) - 2\mu h \omega_n} W_n(M) \mathrm{e}^{-\mathrm{i}\omega_n t} \right.\right.$$
$$\left.\left. - \frac{\langle f, W_n^* \rangle^*}{\Lambda_n'^*(\omega_n) - 2\mu h \omega_n^*} W_n^*(M) \mathrm{e}^{+\mathrm{i}\omega_n^* t} \right] \right\}. \quad (18)$$

With the assumption that $\tilde{W}(M,t)$ is a twice differentiable function, the convolution products reduce to integrals and the numerical computation is rather straightforward. Details are given in Ref. [2].

2.4. Comparison of numerical predictions with experimental results

The efficiency of the numerical method which is presented in this paper has been tested on a very simple experiment. The Laboratoire de Mécanique et d'Acoustique has a semi-anechoic room connected to an anechoic one by an aperture. A clamped plate is set in this aperture. A small ball is suspended at the extremity of a nylon thread a few centimetres in front of the plate. The ball is moved apart from its equilibrium position and then released. It thus gives the plate a short impulse, the strength of which is set to obtain a sufficiently loud acoustic signal. The acoustic measurements are conducted in the semi-anechoic room. The plate can be considered, with a rather fair accuracy, as clamped into a perfectly rigid baffle.

The plate is made of stainless steel. Its dimensions are $0.700 \times 0.546 \times 0.005\ \mathrm{m}^3$. For the numerical predictions, we have adopted a density of $7800\ \mathrm{kg/m}^3$, Young's modulus of 2.1×10^{11} Pa and a Poisson ratio of 0.33. With these numerical data, the computed resonance frequencies are in good agreement with the experimental ones.

The centre of the plate is used as the origin of the co-ordinate system. Two balls have been used: a plexiglass ball which excites the plate at the point ($x = -0.075$ m, $y = 0.0025$ m); and a hard rubber ball which impacts the plate at the point ($x = -0.115$ m, $y = 0.0025$ m). For both

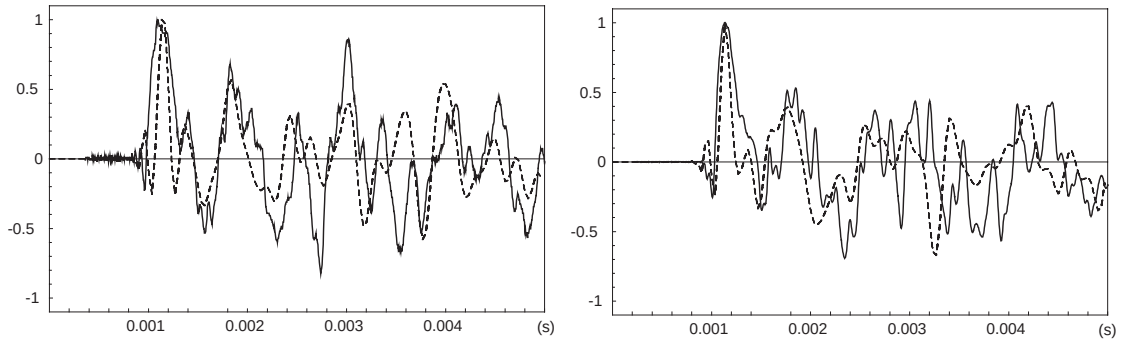

Fig. 2. Acoustic pressure radiated by a steel plate hit by a plexiglass ball (left) or a rubber ball (right): experimental (continuous line) versus calculated (dashed line) results.

excitations, the transient acoustic pressure is recorded at point ($x = -0.110$ m, $y = 0.2625$ m, $z = 0.265$ m). Both impulses have been modelled as a force $\tilde{f}(t)$, with total duration $2\vartheta_1 = 10^{-4}$ s, and with the following time dependence:

$$\tilde{f}(t) = \begin{cases} 1 - \cos\left(\dfrac{2\pi t}{\vartheta_1}\right) & \text{for } 0 < t < \vartheta_1/2, \\ 1 + \cos\left(\dfrac{2\pi(t-\vartheta_1)}{3\vartheta_1}\right) & \text{for } \vartheta_1/2 < t < 2\vartheta_1. \end{cases} \tag{19}$$

The experimental signals and the numerical ones have been adjusted so that the amplitude of the first peak is equal to 1. Because it has not been possible to record exactly the impact time, each experimental curve has been shifted so that the maximum of its first peak coincides with the maximum of the first peak of the numerical curve. This enables to compare the experiments with the predictions. Fig. 2 shows the first 5 ms of the recorded signals versus the computed ones. A fair agreement can be observed despite the fact that this experiment has been conducted in a rather simple way, the aim being just to get an idea of the possibility to predict the phenomenon. When the time increases besides the first milliseconds, the signal is much more regular. It corresponds to the "reverberated" oscillations of the plate and shows the beats produced by the time interferences between the different modes of the plate.

3. Computation of the coupling term β_ω

In this section and the following, we consider a rectangular plate with boundaries which can be either clamped or simply supported, which occupies the domain $\Sigma = [-L_x < x < +L_x; -L_y < y < +L_y]$ with $L_y > L_x$.

The first step is to define the basis functions U_m as products of one-dimensional functions $U_m(x,y) = v_{m_x}(x/2L_x)v_{m_y}(y/2L_y)$. Let $v_p(\xi)$ represent the in vacuo resonance modes of a perfectly elastic beam extending from $\xi = -1/2$ to $\xi = +1/2$, and satisfying the same boundary conditions as the plate in the ξ direction (clamped or simply supported at both ends of the beam). The set of functions $v_{m_x}(x/2L_x)v_{m_y}(y/2L_y)$ is a convenient basis of orthogonal functions. They are chosen with a $\mathbf{L}^2$-norm equal to 1.

By convention, the indices m_x and m_y are equal to the total number of nodal lines inside the plate domain, in the x and y directions, respectively: they start from 0. Since it is easier to index the basis functions with a unique number, we have chosen to class them by groups in which the total number of nodal lines is constant. Thus the index m of functions $U_m(x,y) \coloneqq v_{m_x}(x)v_{m_y}(y)$ is related to the indices m_x and m_y as shown in Table 1. It is well known that when such a basis is

Table 1
Numbering of the basis functions $U_m = v_{m_x}v_{m_y}$

m_x	0	0 1	0 1 2	0 1 2 3	⋯
m_y	0	1 0	2 1 0	3 2 1 0	⋯
m	1	2 3	4 5 6	7 8 9 10	⋯
Group #	1	2	3	4	…

used, an in vacuo resonance mode which has m_x nodal lines in one direction and m_y in the other has a strongly dominant component on the function $v_{m_x}(x/2L_x)v_{m_y}(y/2L_y)$. This property remains true when fluid-loading is present and, thus, modes can always be identified by a couple of integers.

In numerical approximations, the maximum number M of basis functions used is chosen so that U_M has almost the same density of nodal lines in x and y; more precisely, if we choose a maximum number N_x of nodal lines in the x direction, the maximum number N_y in the y direction is the closest integer to N_xL_y/L_x. As a consequence, in the highest order groups, some functions may be missing (for example, with $N_x = N_y = 2$, the functions $v_0(x)v_3(y)$ and $v_3(x)v_0(y)$ are not taken into account). This choice is, of course, arbitrary but quite reasonable—at least in the authors' opinion. The total number of basis functions is $M = (N_x + 1)(N_y + 1)$.

3.1. Numerical calculation of the plate terms

In Eq. (14), the first two terms, $\mathscr{A}(U_m, U_q^*)$ and $\int(1 + \varepsilon)U_m Uq$, involve the plate properties only. If the plate has a constant thickness, they are calculated analytically. For varying thickness, the terms which are independent of ε are calculated analytically, while the other ones are approximated by a Simpson's algorithm.

The reason to choose such an algorithm is that the functions involved are very close to periodic functions for which Simpson's algorithm is well known to provide accurate results. We have adopted the same number n_s of Simpson's points for all the integrations: $(N_x + 1)n_s$ intervals in the x direction and $(N_y + 1)n_s$ intervals in the y direction. For a periodic function, this corresponds to divide each half-period into n_s intervals. The choice of $n_s = 4$ proved to be quite sufficient: an increase of these numbers does not change the results by a significant amount (less than 10^{-5} on the resonance frequencies).

3.2. Numerical calculation of the coupling term

As in the papers cited in introduction, simplifications are introduced by taking advantage of the properties of the functions to be integrated: because of symmetry properties, most of the integrals are equal to 0 and, for the others, the integration domain can be reduced to a quarter of the plate. But the main numerical difficulty comes from the singularity of the Green's kernel. The solution proposed here can be easily used for any structure—plates, shells or three-dimensional bodies.

Let us write the explicit form of the coupling term as follows:

$$\beta_\omega(U_m, U_q^*) = -\int_\Sigma U_m(P) I_q(P)\,\mathrm{d}P,$$

$$\text{where} \quad I_q(P) = \int_\Sigma U_q(P') g(|x - x'|, |y - y'|)\,\mathrm{d}P'$$

$$\text{and} \quad g(|x - x'|, |y - y'|) = \frac{\mathrm{e}^{\mathrm{i}kr(P,P')}}{\pi r(P, P')}. \tag{20}$$

First note that the functions $v_p(\xi)$ are either even or odd in ξ. Let us recall that the function $U_m(x, y)$ is odd in x (respectively in y) if m_x (respectively m_y) is odd, and even if m_x (respectively

m_y) is even. So, any basis function has the following property:

$$U_m(x,y) = (-\text{sign } x)^{m_x}(-\text{sign } y)^{m_y} U_m(|x|,|y|). \tag{21}$$

Because Green's kernel g in Eq. (20) is a function of $|x-x'|$ and $|y-y'|$, the integral I_q has the same parity in x and y as U_q (the proof is very easy). As a consequence, the coupling term is zero unless both functions U_m and U_q have the same parity. This reduces highly the number of terms to be evaluated numerically.

The integral $I_q(P)$ is a smooth function. So, as soon as $I_q(P)$ is known on the set of Simpson's points, the coupling term β_ω can easily be evaluated by the Simpson's algorithm defined in the previous subsection. Furthermore, because of the parity properties of U_m and I_q, the integration can be performed on a quarter of the plate only.

Nevertheless, because of the singularity of Green's kernel g, $I_q(P)$ itself cannot be computed by a Simpson's rule (or any of the most classical algorithms), even if double precision arithmetic is used. We therefore propose an algorithm which combines an analytical approximation and a Simpson's algorithm. Because of parity, the integral $I_q(x,y)$ is expressed as

$$I_q(x,y) = \int_0^{L_x}\int_0^{L_y} U_q(x',y')\bar{g}(x,x',y,y')\,\mathrm{d}x'\,\mathrm{d}y'$$

$$\begin{aligned}\text{with}\quad \bar{g}(x,x',y,y') = {} & g(|x-x'|,|y-y'|) + (-1)^{q_x} g(|x+x'|,|y-y'|) \\ & + (-1)^{q_y} g(|x-x'|,|y+y'|) + (-1)^{q_x+q_y} g(|x+x'|,|y+y'|),\end{aligned} \tag{22}$$

where q_x and q_y are related to q as shown in Table 1. Let δ_x (resp. δ_y) be the interval in the x direction (resp. the y direction) chosen in the Simpson's algorithm. Let $Y(\sigma)$ be the Heaviside function on the rectangle $\sigma = (x-\delta_x/2<x'<x+\delta_x/2; y-\delta_y/2<y'<y+\delta_y/2)$. The function $\bar{g}$ is split into a singular part $\bar{g}_S$:

$$\bar{g}_S = Y(\sigma) g(|x-x'|,|y-y'|) \tag{23}$$

and a regular part $\bar{g}_R$:

$$\begin{aligned}\bar{g}_R(x,x',y,y') = {} & (1 - Y(\sigma)) g(|x-x'|,|y-y'|) + (-1)^{q_x} g(|x+x'|,|y-y'|) \\ & + (-1)^{q_y} g(|x-x'|,|y+y'|) + (-1)^{q_x+q_y} g(|x+x'|,|y+y'|).\end{aligned}$$

The product $U_q\bar{g}_R$ is integrated by the Simpson's algorithm. The contribution of the singular term is approximated by

$$\begin{aligned}&\int_\sigma U_q(x',y')\bar{g}_S(|x-x'|,|y-y'|)\,\mathrm{d}x'\,\mathrm{d}y' \\ &\quad \simeq U_q(x,y)\int_\sigma \bar{g}_S(|x-x'|,|y-y'|)\,\mathrm{d}x'\,\mathrm{d}y'.\end{aligned} \tag{24}$$

This last integral is equal to

$$\begin{aligned}J(x,y) &= \int_{x-\delta_x/2}^{x+\delta_x/2}\int_{y-\delta_y/2}^{y+\delta_y/2} \bar{g}_S(|x-x'|,|y-y'|)\,\mathrm{d}x'\,\mathrm{d}y' \\ &= 4\int_0^{\delta_x/2}\int_0^{\delta_y/2} \bar{g}_S(X,Y)\,\mathrm{d}X\,\mathrm{d}Y,\end{aligned} \tag{25}$$

Table 2
Error on the integration of the singular term $\bar{g}_S$ for two values of n_s

Frequency (Hz)	100	250	500	750	1000
Error in dB for $n_s = 4$	8.0×10^{-4}	5.0×10^{-3}	2.0×10^{-2}	4.5×10^{-2}	8.0×10^{-2}
Error in dB for $n_s = 6$	3.5×10^{-4}	2.2×10^{-3}	8.1×10^{-3}	2.0×10^{-2}	3.5×10^{-2}

which is independent on x and y. Using polar co-ordinates (r, θ), the integral becomes:

$$J = \int_0^{\theta_0} \mathrm{d}\theta \int_0^{\delta_x/\cos\theta} \frac{\mathrm{e}^{\mathrm{i}kr}}{\pi r} r \,\mathrm{d}r + \int_{\theta_0}^{\pi/2} \mathrm{d}\theta \int_0^{\delta_y/\cos(\pi/2-\theta)} \frac{\mathrm{e}^{\mathrm{i}kr}}{\pi r} r \,\mathrm{d}r$$

with

$$\theta_0 = \arctan\frac{L_y}{L_x}$$

$$= \frac{1}{\mathrm{i}k\pi} \int_0^{\theta_0} \left[\exp(\mathrm{i}k\delta_x/\cos\theta) - 1\right] \mathrm{d}\theta + \frac{1}{\mathrm{i}k\pi} \int_{\theta_0}^{\pi/2} \left[\exp(\mathrm{i}k\delta_y/\cos(\pi/2-\theta)) - 1\right] \mathrm{d}\theta. \quad (26)$$

It does not seem possible to obtain an analytical result. Since δ_x and δ_y are small, the terms to be integrated are replaced by the first two terms of their Taylor series

$$\mathrm{e}^{\mathrm{i}kz} - 1 = \mathrm{i}kz - \frac{k^2 z^2}{2} + \mathcal{O}(k^3 z^3). \quad (27)$$

The integral can thus be evaluated analytically: the result is easily obtained with any kind of mathematical software such as Mathematica. The accuracy of this approximation has been tested on several numerical data by comparing the approximated analytical integral with an accurate numerical integration performed with Mathematica which has more than 7 exact digits. The results shown in Table 2 are obtained with the following data: $L_x = 0.35$ m; $L_y = 0.50$ m; $N_x = 7$ and $N_y = 10$ (88 basis functions). With $n_s = 4$, we get $\delta_x = 2.19 \times 10^{-2}$ and $\delta_y = 2.27 \times 10^{-2}$; with $n_s = 6$, we get $\delta_x = 1.67 \times 10^{-2}$ and $\delta_y = 1.52 \times 10^{-2}$. It can be seen in Table 2 that the error obtained with the smallest value of n_s does not exceed 0.08 dB: such an accuracy is in general quite sufficient for acoustic purposes.

4. Computation of the resonance frequencies and modes

4.1. Iterative procedure

We make the following hypothesis. To each in vacuo mode corresponds a fluid-loaded mode which has the same number of nodal lines in the x and y directions. To our knowledge, this assumption is confirmed experimentally. But we do not know if it can be proved. A subsequent assumption is that the order of multiplicity of an in vacuo mode and of the corresponding fluid-loaded mode is the same. For simplicity, in what follows we consider modes with multiplicity order equal to 1.

The resonance frequencies ω_n are the values of the angular frequency for which Eq. (11) or (14) have a non-zero solution. The resonance modes $W_n(M)$ are the corresponding solutions (uniquely defined up to a multiplicative constant).

In practice, the series expansion of W_n is truncated at a finite order, say R, and system (14) is replaced by a system of R equations:

$$\sum_{m=1}^{R} u_n^m \left\{ \mathscr{A}(U_m, U_q^*) - \mu h_0 \omega_n^2 \left[\int_\Sigma (1+\varepsilon) U_m U_q - \frac{\mu_0}{\mu h_0} \beta_{\omega_n}(U_m, U_q^*) \right] \right\} = 0,$$
$$q = 1, 2, \ldots, R. \tag{28}$$

The direct way for evaluating the first R resonance frequencies is to look for the values of ω for which this system has non-zero solutions. A Marquardt's algorithm is well adapted to this problem but requires a large amount of calculations. Nevertheless, as shown in Ref. [13], very accurate results can be obtained.

A more straightforward way, much less time consuming, is to use an iterative procedure which is suggested by noting that the coupling term described by the integral operator β_{ω_n} corresponds, in some way, to a second order effect; the behaviour of the plate is mainly governed by the in vacuo plate operator. In a first step, the in vacuo resonance angular frequencies $\omega_n^{(0)}$ and modes Z_n are computed by solving the classical eigenvalue problem:

$$\sum_{m=1}^{R} u_n^{m(0)} \left\{ \mathscr{A}(U_m, U_q^*) - \mu h_0 \omega_n^{(0)2} \int_\Sigma (1+\varepsilon) U_m U_q \right\} = 0, \quad q = 1, 2, \ldots, R, \tag{29}$$

where the in vacuo modes are approximated by

$$Z_n(M) = \sum_{m=1}^{R} u_n^{m(0)} U_m(M).$$

The main component of Z_n has indexes (n_x, n_y). The system of equations (29) provides R in vacuo resonance frequencies $\omega_n^{(0)}$. The components of each resonance mode are chosen so that its norm is unity. Then, for each resonance frequency of the coupled system, the operator β_{ω_n} in Eq. (28) is replaced by $\beta_{\omega_n^{(0)}}$, leading to a sequence of R classical eigenvalue problems:

$$\sum_{m=1}^{R} u_v^{m(1)} \left\{ \mathscr{A}(U_m, U_q^*) - \Lambda_v^{(1)} \left[\int_\Sigma (1+\varepsilon) U_m U_q - \frac{\mu_0}{\mu h_0} \beta_{\omega_n^{(0)}}(U_m, U_q^*) \right] \right\} = 0,$$
$$q = 1, 2, \ldots, R. \tag{30}$$

This system has R eigenfunctions $W_v^{(1)}$ with a main component of indexes (v_x, v_y). The approximation $W_n^{(1)}$ of the fluid-loaded mode which corresponds to Z_n is the eigenfunction for which the couple (v_x, v_y) is equal to (n_x, n_y).

Let $\Lambda_n^{(1)}$ be the corresponding eigenvalue. A first order approximation of the resonance angular frequency is related to this eigenvalue by

$$\omega_n^{(1)} = \begin{cases} \sqrt{\dfrac{1}{\mu h_0}} \sqrt{\Lambda_n^{(1)}} & \text{if } \Im(\Lambda_n^{(1)}) < 0, \\ -\sqrt{\dfrac{1}{\mu h_0}} \sqrt{\Lambda_n^{(1)}} & \text{if } \Im(\Lambda_n^{(1)}) > 0. \end{cases} \tag{31}$$

This choice ensures that $\omega_n^{(1)}$ has a positive real part as $\omega_n^{(0)}$ does and a negative imaginary part describing a damping.

To estimate the accuracy of this first order approximation, let us define the vectors $V^{(0)}$ and $V^{(1)}$ by

$$V^{(0)} = \sum_q \gamma_q^{(0)} U_q, \quad V^{(1)} = \sum_q \gamma_q^{(1)} U_q,$$

$$\gamma_q^{(0)} = \sum_{m=1}^{R} u_n^{m(0)} \left\{ \mathscr{A}(U_m, U_q^*) - \mu h_0 \omega_n^{(0)2} \left[\int_\Sigma (1+\varepsilon) U_m U_q - \frac{\mu_0}{\mu h_0} \beta_{\omega_n^{(0)}}(U_m, U_q^*) \right] \right\},$$

$$\gamma_q^{(1)} = \sum_{m=1}^{R} u_n^{m(1)} \left\{ \mathscr{A}(U_m, U_q^*) - \mu h_0 \omega_n^{(1)2} \left[\int_\Sigma (1+\varepsilon) U_m U_q - \frac{\mu_0}{\mu h_0} \beta_{\omega_n^{(1)}}(U_m, U_q^*) \right] \right\}. \tag{32}$$

The norm of $V^{(0)}$, (resp. $V^{(1)}$), measures the error made when, in Eqs. (28), the exact solution (u_n^m, ω_n) is replaced by $(u_n^{m(0)}, \omega_n^{(0)})$ (resp. $(u_n^{m(1)}, \omega_n^{(1)})$). A good estimate of the accuracy of the first approximation is given by the ratio $\|V^{(1)}\|/\|V^{(0)}\|$.

As indicated before, $u_n^{m(0)}$ are the components of the in vacuo resonance mode, and $u_n^{m(1)}$ those of the first approximation of the fluid-loaded resonance mode. Because of its construction, $V^{(0)}$ is different from zero.

The procedure is then repeated to obtain a sequence of approximate resonance angular frequencies $\omega_n^{(r)}$ and modes. If the iterative process converges, the successive vectors $V^{(r)}$ tend to zero. The accuracy of the rth approximation is estimated by the ratio $\|V^{(r)}\|/\|V^{(0)}\|$. As it will be seen in the next section, this procedure converges well even for a strong coupling.

Let us recall that expressions (17) and (18) of, respectively, the plate displacement and the acoustic pressure require the value $\Lambda_n'(\omega_n)$ of the derivative of Λ_n with respect to the angular frequency. The successive approximations of the eigenvalues Λ_n allows an approximation of their derivative Λ_n' by a finite difference formula to be obtained.

4.2. The Warburton approximation

A classical approximation for in vacuo plates is due to Warburton (see, for example Ref. [9]): it consists in keeping only the diagonal terms in the resonance mode equation. This implies that each resonance mode is approximated by only one basis function (a product of beam modes). The same approximation can be used for a fluid-loaded plate, and Eq. (28) is replaced by

$$\mathscr{A}(U_m, U_m^*) - \mu h_0 \omega_m^2 \left[\int_\Sigma (1+\varepsilon) U_m U_m - \frac{\mu_0}{\mu h_0} \beta_{\omega_m}(U_m, U_m^*) \right] = 0,$$
$$m = 1, 2, \ldots, R. \tag{33}$$

Here again the iterative procedure previously described enables to obtain, for each mode, a sequence of angular frequencies $\omega_n^{(r)}$ which converges to the solution of Eq. (33) but, of course, not to the exact resonance frequency. Nevertheless, the advantage of this approximation is to divide the computation time by a factor 2, or so, and to give a rather accurate result.

The accuracy of the approximation can be greatly improved by constructing the Warburton approximation on the in vacuo modes of the plate instead of on the basis functions U_m. Eq. (28)

becomes

$$\sum_{m=1}^{R} u_n^m \left\{ \left[\omega_n^{(0)2} - \omega_n^2\right] \int_\Sigma (1+\varepsilon) Z_m Z_q - \omega_n^2 \frac{\mu_0}{\mu h_0} \beta_{\omega_n^{(0)}}(Z_m, Z_q^*) \right\} = 0,$$
$$q = 1, 2, \ldots, R. \tag{34}$$

Taking the first iteration of the Warburton's approximation of this equation leads to

$$\omega_m^2 \simeq \omega_m^{(0)2} \left[1 - \frac{\mu_0}{\mu h_0} \frac{\beta_{\omega_n^{(0)}}(Z_m, Z_m^*)}{\int_\Sigma (1+\varepsilon) Z_m Z_m} \right]^{-1}. \tag{35}$$

4.3. The light-fluid approximation

Assuming a weak fluid-loading, that is $\mu_0/\mu h_0 \ll 1$, we obtain [8] the first order light-fluid approximation:

$$\omega_m^2 \simeq \omega_m^{(0)2} \left[1 + \frac{\mu_0}{\mu h_0} \frac{\beta_{\omega_n^{(0)}}(Z_m, Z_m^*)}{\int_\Sigma (1+\varepsilon) Z_m Z_m} \right]. \tag{36}$$

Comparing Eqs. (35) and (36), it is easily seen that Eq. (36) is an approximation of Eq. (35) if the ratio within brackets is smaller than 1, which is so for a weak coupling.

The classical approximation of "added mass", as it is described in Ref. [10], is a rough analytical estimation of the integrals involved in Eq. (35) which has the advantages to clearly describe the physical phenomenon and to give an idea of the effect of the fluid without the use of a computer.

5. Numerical examples

The methods previously described have been tested on various examples, among them a clamped steel plate with dimensions $2L_x = 0.350$ m and $2L_y = 0.500$ m. The main results presented here were obtained for a constant thickness equal to $h_0 = 0.005$ m. Additional results presented in Section 5.4 correspond to a varying thickness given by

$$h = h_0[1 + \varepsilon(x, y)]$$
$$= h_0 \left[1 + \frac{1}{14} \left(\frac{x}{L_x} + 1 \right)^2 \cos(\pi x / L_x) \left(\frac{y}{L_y} + 1 \right)^2 \cos(\pi y / L_y) \right], \tag{37}$$

with $h_0 = 0.005$ m. The maximum of $\varepsilon(x, y)$ is 0.5, that is $h_0 < h < 1.5\ h_0$.

The material has a density $\mu = 7800$ kg/m^3, Young's modulus $E = 2 \times 10^{11}$ Pa and a Poisson's ratio $v = 0.3$.

The fluid is either air with $\mu_0 = 1.3$ kg/m^3 and $c_0 = 340$ m/s; or water with $\mu_0 = 1000$ kg/m^3 and $c_0 = 1500$ m/s.

All computations are conducted with 20 basis functions which have up to 3 nodal lines parallel to the y-axis and up to 4 nodal lines parallel to the x direction. Note that, because of this choice,

Table 3
Resonance frequency of mode 2-3 in air: convergence of the iterative procedure

In vacuo plate	$f^{(0)} = 2437.2$ Hz
Air-loaded plate	$f^{(i)}$ (in Hz)
1st iteration	2435.3 (1−i0.0012617)
2nd iteration	2435.3 (1−i0.0012664)
3rd iteration	2435.3 (1−i0.0012665)
4th iteration	2435.3 (1−i0.0012665)
5th iteration	2435.3 (1−i0.0012665)
$\|\|V^{(5)}\|\|/\|\|V^{(0)}\|\|$	0.20580×10^{-11}

Table 4
Resonance frequency of mode 2-3 in water: convergence of the iterative procedure

In vacuo plate	$f^{(0)} = 2437.2$ Hz
Water-loaded plate	$f^{(i)}$ (in Hz)
1st iteration	1615.5 (1−i0.00026924)
2nd iteration	1629.6 (1−i0.00041743)
3rd iteration	1629.5 (1−i0.00041429)
4th iteration	1629.5 (1−i0.00041431)
5th iteration	1629.5 (1−i0.00041433)
$\|\|V^{(5)}\|\|/\|\|V^{(0)}\|\|$	0.82941×10^{-9}

some resonance modes can be missing in the upper part of the spectrum, but this does not matter for the present purpose.

The last subsection is devoted to the computation of the transient response of a plate in air.

5.1. Convergence of the iterative procedure

The first result is to show that the iterative procedure converges. For this purpose, five iterations have been calculated. Tables 3 and 4 present the successive approximations of the resonance frequency of the mode (3-2) in air and in water. In both cases, the in vacuo resonance frequency is used as the initial guess.

First of all, it must be noticed that the convergence test—$||V^5||/||V^0||$—is of order 10^{-12} in air, and 10^{-10} in water. This confirms that the resonance frequencies obtained are close to the exact value, that is the value for which Eq. (28) is satisfied.

For the plate in air, it appears that three iterations are quite sufficient. With water-loading, the real part of the resonance frequency does not change after the third iteration and the imaginary

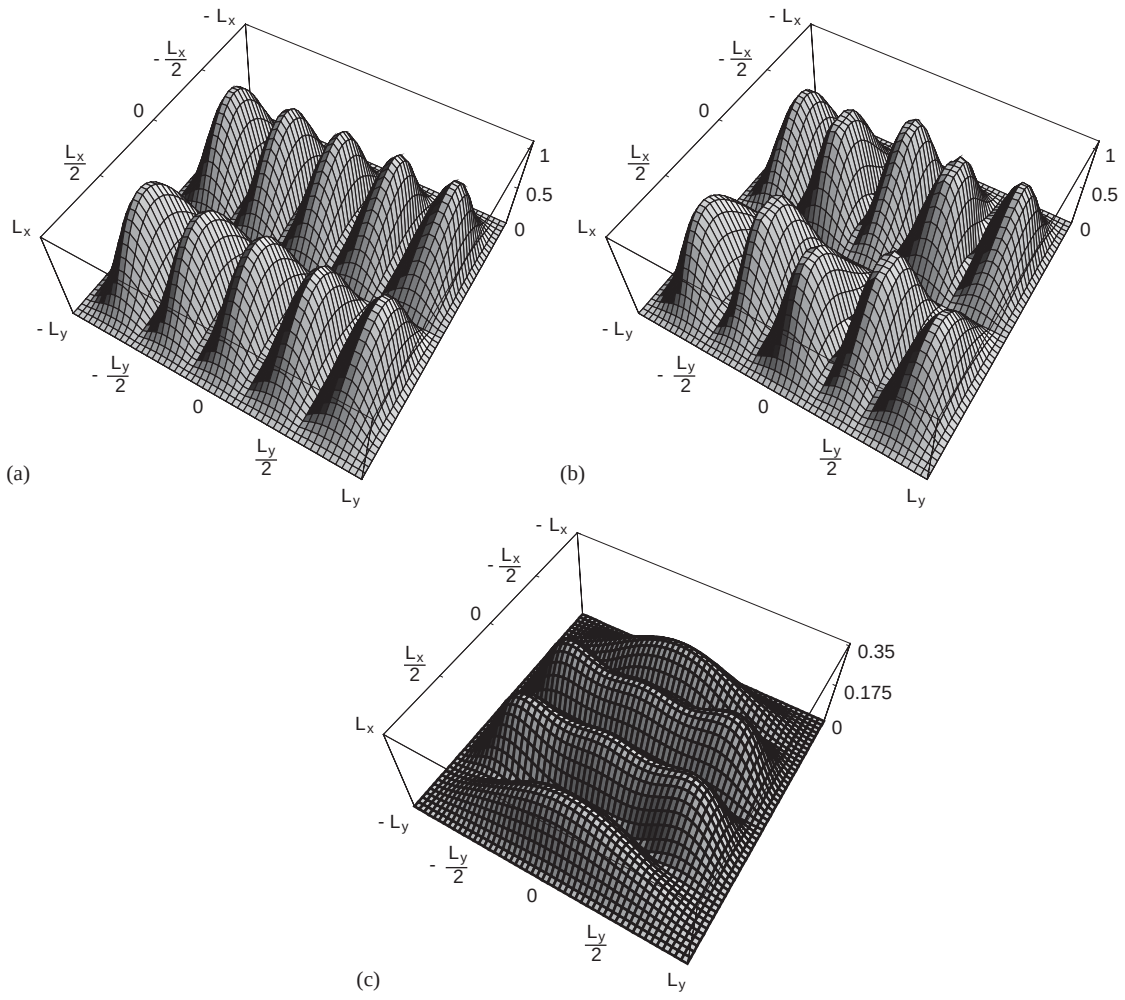

Fig. 3. Mode 1-4: (a) in vacuo mode; (b) water-loaded mode; (c) difference between the in vacuo and the water-loaded modes.

part presents a variation on the fifth digit only: so, here again, three iterations provide a conveniently accurate result.

In Tables 3 and 4, the results are presented with five digits for the resonance frequencies and the damping factors to show clearly how the procedure converges. But, of course, for engineering applications, four digits on the resonance frequencies and two on the damping factors seem quite sufficient.

Fig. 3 (mode 1-4) and Fig. 4 (mode 3-2) show the absolute value of: the in vacuo mode shape (a), the water-loaded mode shape (b) and of the difference between these two functions (c). It appears that the difference (absolute value) between the fluid-loaded mode and the in vacuo one increases with the damping, that is with the amount of energy that the mode radiates: it is less than 0.35 for the mode 1-4, and less that 0.1 for the mode 3-2.

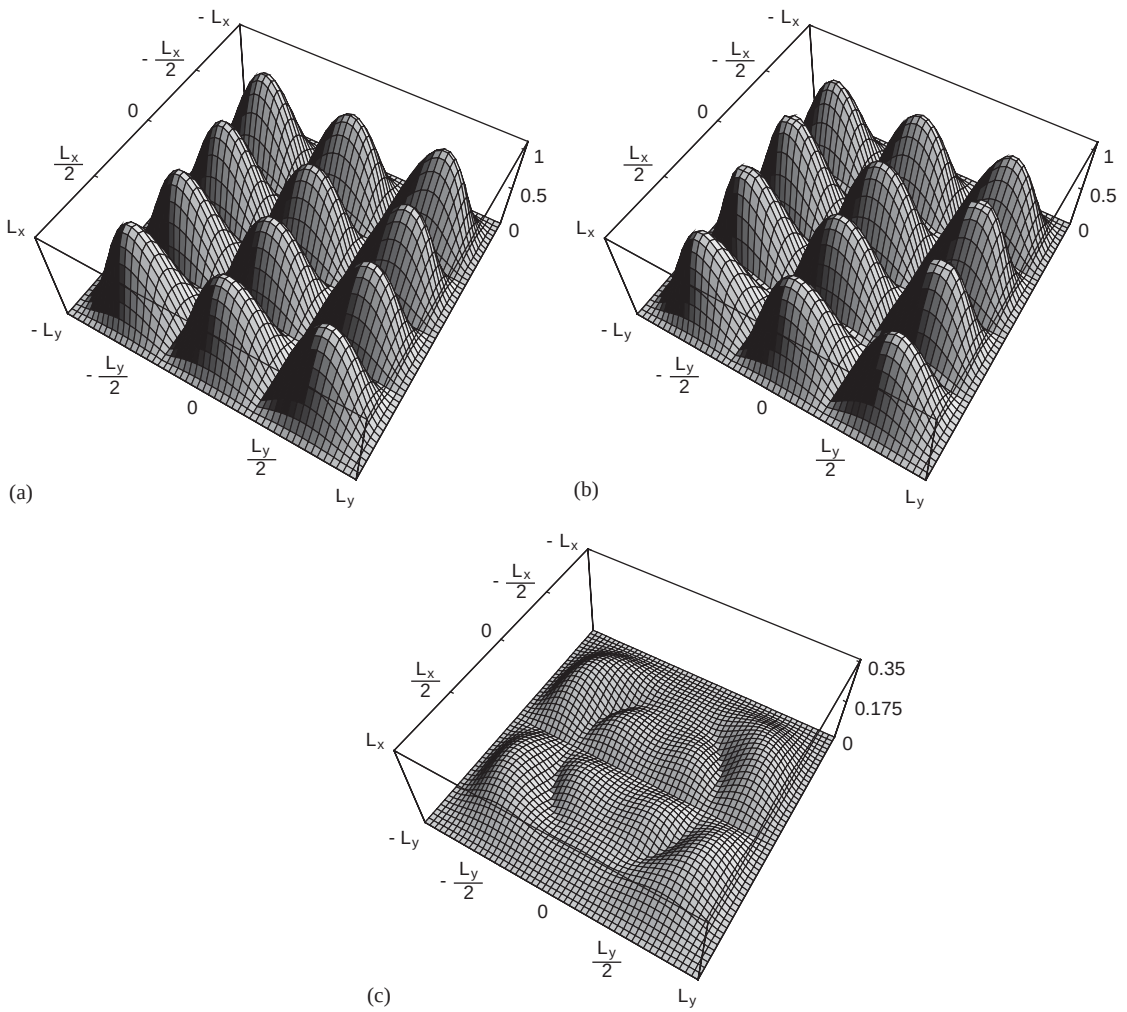

Fig. 4. Mode 3-2: (a) in vacuo mode; (b) water-loaded mode; (c) difference between the in vacuo and the water-loaded modes.

5.2. Comparison between the solution of the exact equations and the Warburton's approximation

Tables 5 and 6 present the first 20 resonance frequencies computed by the iterative method applied to the exact equations and applied to the Warburton's approximate equations. The fifth column is the norm of the difference between the fluid-loaded plate Warburton's approximation of the modes $W_n^{(W)}$ and the in vacuo ones Z_n.

The first comment is that the Warburton's approximation provides a reasonable accuracy. Nevertheless, it is not quite satisfactory to find frequencies in air slightly higher than the in vacuo ones. The second comment is that in air the resonance modes remain almost unchanged (a well-known result), while in water the difference is not negligible.

Table 5
Resonance frequencies (in Hz) for the plate in air: iterative procedure applied to exact equations and to the Warburton's approximated equations; light-fluid approximation

Mode index	Vacuum	Air (exact)	Air (Warburton)	$\|\|Z_n - W_n^{(W)}\|\|$	Light-fluid approximation
0 0	275.2	274.1(1−i0.00204)	274.9(1−i0.00200)	0.00031	274.1(1−i0.00208)
0 1	440.0	438.7(1−i0.00077)	440.4(1−i0.00075)	0.00027	438.7(1−i0.00079)
1 0	663.8	662.2(1−i0.00104)	664.6(1−i0.00101)	0.00031	662.2(1−i0.00105)
0 2	715.2	713.7(1−i0.00047)	716.5(1−i0.00048)	0.00131	713.6(1−i0.00048)
1 1	817.2	815.4(1−i0.00077)	818.8(1−i0.00074)	0.00033	815.4(1−i0.00079)
1 2	1076.8	1074.7(1−i0.00068)	1078.2(1−i0.00066)	0.00065	1074.6(1−i0.00069)
0 3	1093.6	1091.7(1−i0.00044)	1095.7(1−i0.00045)	0.00150	1091.7(1−i0.00045)
2 0	1252.7	1250.7(1−i0.00088)	1254.3(1−i0.00088)	0.00081	1250.6(1−i0.00089)
2 1	1403.3	1401.1(1−i0.00090)	1405.3(1−i0.00089)	0.00096	1401.0(1−i0.00091)
1 3	1443.6	1441.1(1−i0.00075)	1444.8(1−i0.00075)	0.00082	1441.1(1−i0.00078)
0 4	1571.2	1568.6(1−i0.00066)	1573.9(1−i0.00066)	0.00268	1568.5(1−i0.00068)
2 2	1656.0	1653.5(1−i0.00099)	1654.7(1−i0.00098)	0.00252	1653.5(1−i0.00101)
1 4	1911.6	1908.8(1−i0.00107)	1915.0(1−i0.00106)	0.00100	1908.8(1−i0.00110)
2 3	2017.2	2014.6(1−i0.00116)	2009.1(1−i0.00116)	0.00059	2014.6(1−i0.00119)
3 0	2038.6	2036.4(1−i0.00114)	2040.9(1−i0.00117)	0.00068	2036.3(1−i0.00117)
3 1	2188.5	2186.3(1−i0.00120)	2192.2(1−i0.00122)	0.00051	2186.3(1−i0.00123)
3 2	2437.2	2435.3(1−i0.00127)	2438.0(1−i0.00129)	0.00054	2435.3(1−i0.00129)
2 4	2477.7	2475.6(1−i0.00134)	2468.6(1−i0.00134)	0.00047	2475.7(1−i0.00136)
3 3	2794.5	2793.1(1−i0.00125)	2785.6(1−i0.00127)	0.00028	2793.2(1−i0.00127)
3 4	3247.2	3246.6(1−i0.00104)	3236.3(1−i0.00108)	0.00016	3246.7(1−i0.00107)

5.3. *The light-fluid approximation*

The light-fluid approximation requires some more computations than the first order Warburton's approximation. Indeed, in expression (36), the term $\beta_{\omega_n}(0)(Z_m, Z_m^*)$ contains the in vacuo resonance modes which are expressed as a truncated series of the basis functions U_m. The results presented in Table 5 are obtained for the first 20 air-loaded resonances with in vacuo modes computed with 20 basis functions (product of beam modes). This approximation is quite good. The error on the real part of the resonance frequencies does not exceed 1.4×10^{-3}; the error on the relative damping is less than 4×10^{-2}. This accuracy is in general quite sufficient for acoustical engineering purposes.

5.4. *Plate with variable thickness*

The relative variation $\varepsilon(x, y)$ of the plate thickness, as defined in Eq. (37) is represented on Fig. 5. Compared to the constant thickness plate, the resonance frequencies of the plate (in vacuo or fluid-loaded) are higher. This comes from an increase of the mean plate rigidity induced by the increase of the mean thickness. Table 7 presents the first 20 resonance frequencies of the plate in air and in water (20 basis functions, five iterations).

Figs. 6 and 7 present the modes (1-4) and (3-2) in air and in water. The influence of the thickness variation on the in vacuo modes as well as on the modes in air is quite small. But in

Table 6
Resonance frequencies (in Hz) for the plate in water: iterative procedure applied to the exact equations and to the Warburton approximation

Mode Index	Vacuum	Water (exact)	Water (Warburton)	$\|\|Z_n - W_n^{(W)}\|\|$
0 0	275.2	94.6 (1−i0.01681)	95.4 (1−i0.01627)	0.02912
0 1	440.0	202.4 (1−i0.00011)	203.3 (1−i0.00017)	0.02442
1 0	663.8	329.5 (1−i0.00034)	203.1 (1−i0.00042)	0.02930
0 2	715.2	371.2 (1−i0.00839)	358.3 (1−i0.02375)	0.19230
0 1	817.2	441.5 (1−i0.00027)	442.3 (1−i0.00006)	0.02673
1 2	1076.8	624.4 (1−i0.00001)	620.3 (1−i0.00064)	0.07404
0 3	1093.6	628.6 (1−i0.00158)	616.0 (1−i0.00294)	0.15805
2 0	1252.7	709.6 (1−i0.01395)	671.4 (1−i0.05011)	0.23586
2 1	1403.3	841.6 (1−i0.00094)	824.8 (1−i0.00346)	0.13886
1 3	1443.6	891.2 (1−i0.00061)	881.2 (1−i0.00000)	0.07679
0 4	1571.2	968.3 (1−i0.00651)	946.4 (1−i0.02934)	0.24222
2 2	1656.0	1042.1 (1−i0.00057)	1023.1 (1−i0.01405)	0.19341
1 4	1911.6	1237.3 (1−i0.00141)	1222.9 (1−i0.00201)	0.26060
2 3	2017.2	1322.7 (1−i0.00014)	1290.6 (1−i0.00491)	0.07357
3 0	2038.6	1279.5 (1−i0.00512)	1239.0 (1−i0.01249)	0.31761
3 1	2188.5	1418.0 (1−i0.00004)	1392.2 (1−i0.00140)	0.12869
3 2	2437.2	1629.4 (1−i0.00041)	1599.8 (1−i0.00390)	0.10121
2 4	2477.7	1683.6 (1−i0.00040)	1653.1 (1−i0.00499)	0.06546
3 3	2794.5	1923.4 (1−i0.00105)	1879.7 (1−i0.00198)	0.07298
3 4	3247.2	2292.6 (1−i0.00160)	2244.7 (1−i0.00255)	0.06118

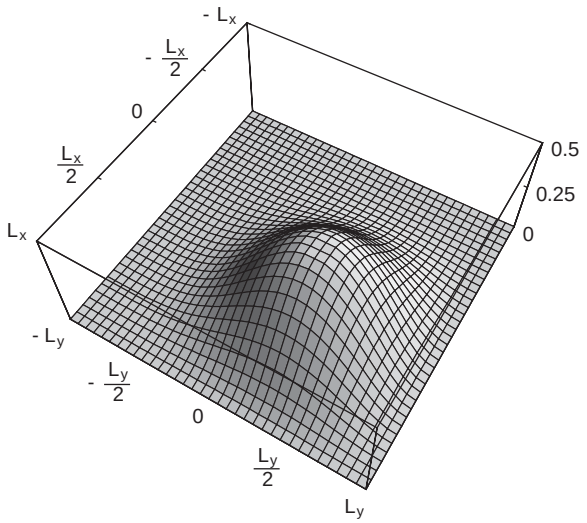

Fig. 5. Relative variation of the plate thickness.

Table 7
Resonance frequencies of the plate with varying thickness in air and water

Mode index	Vacuum	Air	Water
0 0	287.7	286.7 (1−i0.00184)	105.6 (1−i0.01878)
0 1	469.2	467.9 (1−i0.00083)	225.9 (1−i0.00022)
1 0	722.0	720.5 (1−i0.00112)	372.0 (1−i0.00058)
0 2	778.9	777.4 (1−i0.00061)	419.7 (1−i0.00906)
1 1	876.0	874.3 (1−i0.00090)	489.7 (1−i0.00021)
1 2	1148.0	1146.0 (1−i0.00084)	683.5 (1−i0.00036)
0 3	1222.9	1220.9 (1−i0.00069)	733.2 (1−i0.00205)
2 0	1377.5	1375.5 (1−i0.00099)	808.8 (1−i0.01377)
2 1	1553.6	1551.6 (1−i0.00106)	963.4 (1−i0.00346)
1 3	1576.5	1574.3 (1−i0.00103)	1006.3 (1−i0.00019)
0 4	1760.5	1758.1 (1−i0.00111)	1128.7 (1−i0.00520)
2 2	1798.0	1795.9 (1−i0.00114)	1161.1 (1−i0.00101)
1 4	2114.4	2112.5 (1−i0.00132)	1414.2 (1−i0.00420)
2 3	2211.6	2209.8 (1−i0.00124)	1434.2 (1−i0.00012)
3 0	2218.6	2216.8 (1−i0.00120)	1499.8 (1−i0.00223)
3 1	2490.6	2489.6 (1−i0.00110)	1667.0 (1−i0.00376)
3 2	2665.9	2664.9 (1−i0.00112)	1828.4 (1−i0.00050)
2 4	2731.7	2730.9 (1−i0.00113)	1917.2 (1−i0.00100)
3 3	3096.4	3096.1 (1−i0.00090)	2200.5 (1−i0.00132)
3 4	3596.0	3595.9 (1−i0.00066)	2618.5 (1−i0.00204)

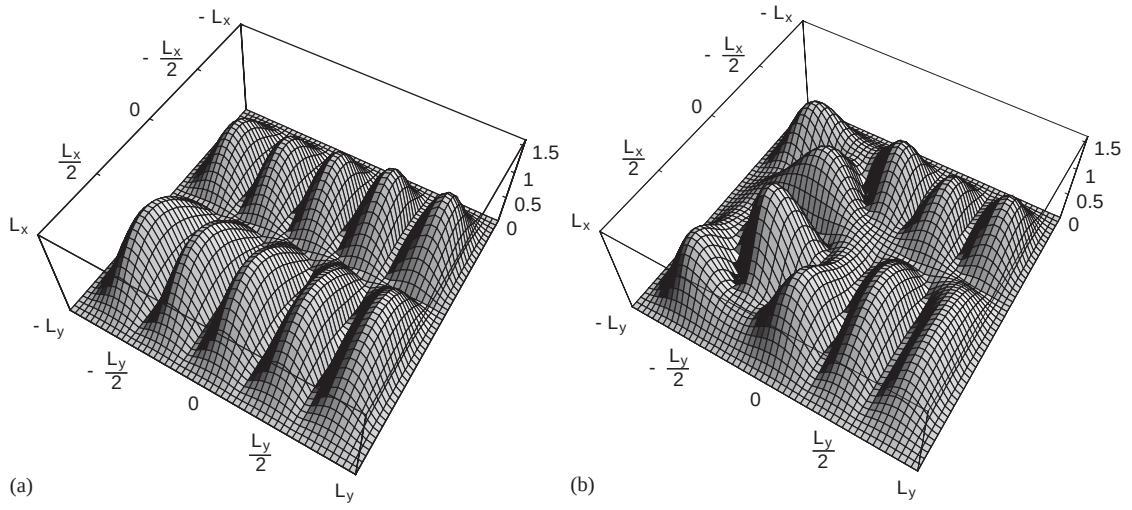

Fig. 6. Variable thickness plate: mode 1-4 in air (a) and in water (b).

water, the variation of the plate thickness can induce a rather large modification of the modes shape. It must be expected that, for strongly radiating modes, the perturbation of the mode shape will be stronger in the thinnest region of the plate. This can be observed on the examples shown: the mode (1-4), which corresponds to a damping factor about 8.5 times the damping factor of the mode (3-2), is much more changed.

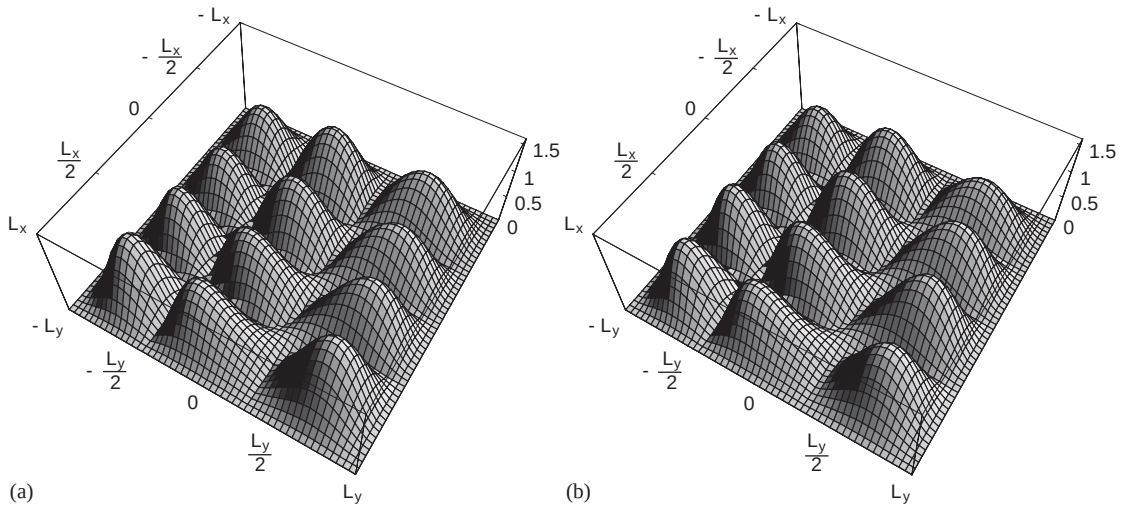

Fig. 7. Variable thickness plate: mode 3-2 in air (a) and in water (b).

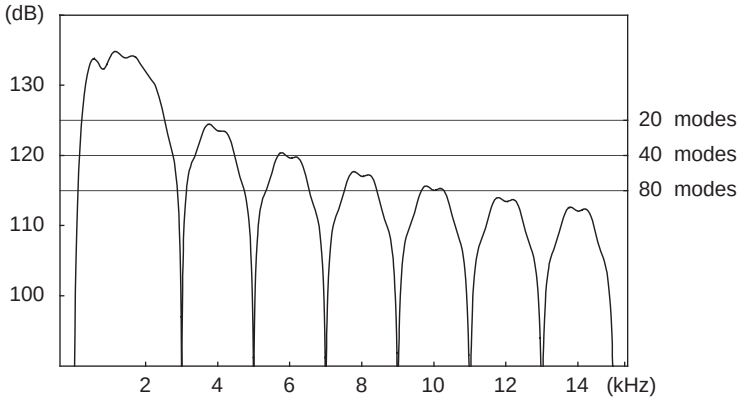

Fig. 8. Spectrum of the second time derivative of the excitation force.

To conclude this subsection, we must say that the iterative procedure converges less rapidly when the thickness of the plate is not constant. This is certainly due to the fact that the in vacuo modes are badly described by a single product of two beam modes. Nevertheless, each modal function has a predominant component and, thus, the characterization of the modes by a pair of indices representing the number of nodal lines in each direction remains meaningful. For more complicated thickness variations, that is certainly not true.

5.5. *Criterion for choosing the number of modes*

When the transient response of a fluid-loaded plate is approximated by a truncated series of resonance modes, it is important to have an a priori idea of the number of modes which is

necessary to reach the desired accuracy. The aim of this section is to suggest an experimental criterion for choosing correctly the number of modes to be accounted for.

We consider the same plate as in Section 2.4. It is excited by an impulsive point force $\tilde{f}(t)$, applied at the point of co-ordinates ($x = 0.165$ m, $y = 0.230$ m), of total duration $\vartheta = 4 \times 10^{-3}$s, and given by

$$\tilde{f}(t) = \frac{1}{\vartheta}\left[1 - \cos\left(\frac{2\pi t}{\vartheta}\right)\right] \quad \text{for } 0 < t < \vartheta. \tag{38}$$

The acoustic pressure is computed at the point ($x = 0.100$ m, $y = 0.000$ m, $z = 0.265$ m).

The first step in choosing the number of modes is to consider the spectrum of the excitation. More precisely, it must be noted that the acoustic pressure involves the integral of the plate acceleration. In the frequency domain, the plate acceleration involves the product of the spectrum of the excitation force by the square of the frequency. The spectrum in $\partial_{t^2}\tilde{f}(t)$ is shown in Fig. 8. Let ω_{max} be the highest angular frequency of the resonance modes used in the approximation of the acoustic pressure. The result is exact if the spectrum of the second time derivative of the excitation force is zero for $\omega > \omega_{max}$. Unfortunately, this is never the case for an excitation of finite duration. Nevertheless, the approximation will be accurate enough if this spectrum can be considered as negligible for frequencies higher than ω_{max}. In Fig. 8, the three horizontal lines correspond to neglecting the contribution of the frequencies which are 10, 15 and 20 dB lower than the maximum level of the spectrum. This corresponds to accounting for 20, 40 and 80 modes respectively. Fig. 9 shows the first 5 ms of the three truncated series. It is obvious that the crudest approximation (20 modes) will not be sufficient in any practical case. But the difference between the other two approximations is quite small. Nevertheless, the final choice of the number of modes to be accounted for depends on the use which is made of the numerical predictions. For example, the predicted acoustic pressure radiated by a structure can be used to conduct psychoacoustics experiments (annoyance due to a noise, acoustic comfort in a vehicle, etc.) [14–16]. In that case,

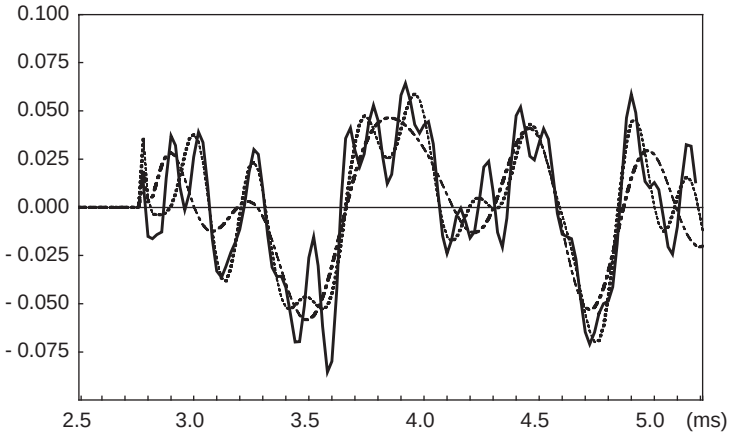

Fig. 9. Approximation of the acoustic pressure by a truncated series: 20 modes (dashed), 40 modes (doted) and 80 modes (solid).

the number of modes must be increased until the difference between two successive approximations cannot be detected by ear.

6. Conclusion

This paper is concerned with the numerical aspects of the computation of the response of a fluid-loaded structure expressed as a series of the fluid-loaded resonance modes.

The main part is dedicated to the computation of the resonance frequencies and modes. From a numerical point of view, the most time-consuming task is to compute the resonance frequencies (and modes, in the case of a strong coupling). This means that when they are known, the response of the structure can be evaluated quite easily for any kind of excitation. Three methods (iteration, Warburton approximation, perturbation) are proposed and compared, for both weak and strong coupling, on numerical simulations. These simulations show in particular, that the iterative method converges rapidly even for a strong coupling. We do not know how to obtain a rigorous proof of this convergence. Anyhow, it is probably related to the following point. The response of the structure is the solution of an equation which includes a differential operator (corresponding to the structure or the in vacuo operator) and an integral operator which describes the fluid-loading. Because it is integral, the fluid-loading operator is a priori small compared with the differential operator, even for strong coupling. This is why the classical approximations (see, for example Ref. [10]) are so powerful. Let us also point out that the convergence of the iterative method will not depend on the choice of the basis functions.

The numerical tests show that for a weak loading the shape of the resonance modes is quite close to the shape of the in vacuo modes, but the damping of the resonance frequencies cannot be neglected, at least for the first ones. This is a well-known result. Another result is that the Warburton's approximation, which is known to be powerful to compute the in vacuo frequencies, is still efficient in the case of a fluid loading. Nevertheless, its accuracy decreases as the influence of the fluid increases.

Another numerical aspect studied here is the computation of the coupling term which must be evaluated accurately because it corresponds to the damping of the resonance frequencies.

The last aspect presented is the choice of the number of modes to be taken into account to predict correctly the sound pressure in the case of a short-duration excitation. An example is shown in this paper. The criterion depends on the accuracy needed in the evaluation of the sound pressure. It should be noticed that prediction methods are now used to study the perceptive properties of sounds radiated by vibrating structures, in order to define comfort and annoyance criteria. The accuracy must be determined by series of subjective tests, where simulated sounds and recorded sounds are compared.

In the first part of this paper, a comparison between numerical simulations and experimental results is shown in the case of a baffled thin plate hit by a small ball. This experiment will be carried out again with a better adapted set-up. It is quite similar to the experiment described in Ref. [17], where the influence of the inelasticity of the phenomenon is taken into account.

Let us finally point out that the methods presented here in the case of a baffled plate can be used similarly for more complex structures.

Appendix A. Nomenclature

$\sim$	functions of time
M	point on the plate
Q	point in the fluid
$\mathrm{sgn}(z)$ or $\mathrm{sign}\, z$	sign of z
$Tr^{+}P(M) = \lim_{z>0\to 0} P(Q)$	the co-ordinates of Q being x, y, z
$Tr^{-}P(M) = \lim_{z<0\to 0} P(Q)$	the co-ordinates of Q being x, y, z
$\tilde{F}(t, M) = \tilde{\psi}(t) f(M)$	force on the plate, as a function of time
$\tilde{W}(M, t)$	displacement as a function of time
$\tilde{P}(M, t)$	sound pressure as a function of time
$\tilde{\tilde{P}}$	jump of $P(M, t)$ across the plane $z = 0$
ω	angular frequency
$\theta(\omega)$	Fourier transform of any function $\tilde{\theta}(t)$
$\tilde{\mathscr{G}}(t, S, M)$	the Green's function for the wave equation with homogeneous Neumann conditions on $z = 0$
$\mathscr{G}_{\omega}(S, M)$	the Green's function for the Helmholtz equation with homogeneous Neumann conditions on $z = 0$
$u \otimes \delta_{\Sigma}$	tensor product of function u by distribution δ on surface Σ
$\beta_{\omega}(W, U)$	coupling term
$\Lambda_n(\omega)$ and $\hat{W}_n(\omega, M)$	eigenvalues and eigenmodes of the fluid-loaded plate
ω_n and $W_n(M)$	resonance angular frequencies and modes of the fluid-loaded plate
$W_n(M) = \sum_{m=1}^{\infty} u_n^m U_m(M)$	expansion of the nth resonance mode in terms of the basis functions U_m
(U_m), $m = 1, 2, \ldots, \infty$	a basis of the space $\mathbf{H}(\Sigma)$ with $U_m(x, y) = v_p(x) v_q(y)$
$v_p(\xi)$	resonance mode of the in vacuo beam
N_x and N_y	number of nodal lines in x and y
$g(\lvert x - x'\rvert, \lvert y - y'\rvert)$, $\bar{g}_S$ and $\bar{g}_R$	Green's kernel in the coupling term, its singular part and its regular part
$\omega_n^{(0)}$	nth resonance frequency of the in vacuo plate
$Z_n(M) = \sum_{m=1}^{R} u_n^{m(0)} U_m(M)$	nth resonance mode of the in vacuo plate expressed as a series of basis functions
$\Lambda_n^{(j)}$	jth iteration of Λ_n
$\omega_n^{(j)}$	jth iteration of ω_n
$V^{(j)}$	jth iteration of a test vector used to check the convergence of the iteration process

References

[1] P.J.T. Filippi, D. Habault, P.-O. Mattei, C. Maury, The role of the resonance modes in the response of a fluid-loaded structure, *Journal of Sound and Vibration* 239 (4) (2001) 639–663.

[2] D. Habault, P.J.T. Filippi, On the transient response of a fluid-loaded structure represented by a series of resonance modes, *Journal of Sound and Vibration* 259 (5) (2003) 1269–1275.

[3] M. Amabili, G. Frosali, M.K. Kwak, Free vibrations of annular plates coupled with fluids, *Journal of Sound and Vibration* 191 (5) (1996) 825–846.
[4] R.A. Mangiarotty, Acoustic radiation damping of vibrating structures, *Journal of the Acoustical Society of America* 35 (3) (1963) 369–377.
[5] S. Snyder, N. Tanaka, Calculating total acoustic power output using modal radiation efficiencies, *Journal of the Acoustical Society of America* 97 (1995) 1702–1709.
[6] W.L. Li, H.J. Gibeling, Determination of the mutual radiation resistances of a regular plate and their impact on the radiated sound power, *Journal of Sound and Vibration* 229 (5) (2000) 1113–1133.
[7] W.L. Li, An analytical solution for the self- and the mutual radiation resistances of a rectangular plate, *Journal of Sound and Vibration* 245 (1) (2001) 1–16.
[8] D. Habault, P.J.T. Filippi, Light fluid approximation for sound radiation and diffraction by thin elastic plates, *Journal of Sound and Vibration* 213 (2) (1998) 333–374.
[9] A.W. Leissa, *Vibration of Plates*, NASA, Washington DC, 1969.
[10] F. Fahy, *Sound and Structural Vibration*, Academic Press, London, 1985.
[11] M.C. Junger, D. Feit, *Sound, Structures and their Interaction*, Acoustical Society of America, 1993.
[12] C. Bardos, M. Concordel, G. Lebeau, Extension de la théorie de la diffusion pour un corps élastique immergé dans un fluide. Comportement asymptotique des résonances, *Journal d'Acoustique* 2 (1989) 31–38.
[13] C. Maury, P.J.T. Filippi, Transient acoustic diffraction and radiation by an axisymmetrical elastic shell: a new statement of the basic equations and a numerical method based on polynomial approximations, *Journal of Sound and Vibration* 239 (4) (2001) 639–663.
[14] S. Meunier, D. Habault, G. Canévet, Auditory evaluation of sound signals radiated by a vibrating surface, *Journal of Sound and Vibration* 247 (5) (2001) 897–915.
[15] D. Habault, S. Meunier, G. Canévet, P.-O. Mattei, Psychomechanical study of sounds radiated by fluid-loaded vibrating plates, *Forum Acusticum Proceedings*, Sevilla, Spain, 16–20 September 2002.
[16] C. Marquis-Favre, J. Faure, F. Sgard, Coupling of quantitative and qualitative studies of the understanding of mechanical parameter variations influence: application to a radiating plate, *Inter-Noise Proceedings*, Nice, France, August 2000.
[17] Ph. Troccaz, R. Woodcock, F. Laville, Acoustic radiation due to the inelastic impact of a sphere on a rectangular plate, *Journal of the Acoustical Society of America* 108 (5) (2000) 2197–2201.